

STAR FORMATION ACROSS THE TAFFY BRIDGE: UGC 12914/15

Yu Gao¹
 gao@astro.umass.edu
 Ming Zhu^{2,3}
 m.zhu@jach.hawaii.edu
 E. R. Seaquist³
 seaquist@astro.utoronto.ca

ABSTRACT

We present BIMA two-field mosaic CO(1-0) images of the Taffy galaxies (UGC 12914/15), which show the distinct taffy-like radio continuum emission bridging the two spiral disks. Large amounts of molecular gas ($1.4 \times 10^{10} M_{\odot}$, using the standard Galactic CO-to-H₂ conversion applicable to Galactic disk giant molecular clouds [GMCs]) were clearly detected throughout the taffy bridge between the two galaxies, which, as in the more extreme case of HI, presumably results from a head-on collision between the two galaxies. The highest CO concentration between the two galaxies corresponds to the H α source in the taffy bridge near the intruder galaxy UGC 12915. This HII region is also associated with the strongest source of radio continuum in the bridge, and shows both morphological and kinematic connections to UGC 12915. The overall CO distribution of the entire system agrees well with that of the radio continuum emission, particularly in the taffy bridge. This argues for the star formation origin of a significant portion of the radio continuum emission. Compared to the HI morphology and kinematics, which are strongly distorted owing to the high-speed collision, CO better defines the orbital geometry and impact parameter of the interaction, as well as the disk properties (e.g., rotation, orientation) of the progenitor galaxies. Based on the 20cm-to-CO ratio maps, we conclude that the starburst sites are primarily located in UGC 12915 and the H α source in the bridge and show that the molecular gas in the taffy bridge is forming into stars with star formation efficiency comparable to that of the target galaxy UGC 12914 and similar to that in the Galactic disk.

Subject headings: galaxies: individual (UGC 12914/5, VV 254) — galaxies: interactions — galaxies: kinematics and dynamics — galaxies: starburst — galaxies: ISM — radio lines: galaxies

1. INTRODUCTION

Both observational evidence and theoretical perspectives show that galaxy interactions and

mergers are one of the most important processes during the formation and evolution of galaxies. This is true both locally in the nearby universe and, in particular, cosmologically at high-redshifts. Interaction/merger-induced starbursts, nuclear activity, feedback, and other associated phenomena, e.g., gas/dust transformation, infalls and outflows, play a critical role in shaping the interstellar medium (ISM) and intergalactic medium (IGM). Although almost all of the most luminous infrared galaxies (LIGs) and ultraluminous infrared galaxies (ULIGs) are known to be involved

¹University of Massachusetts, Department of Astronomy, LGRT-B 619E, 710 North Pleasant Street, Amherst, MA 01003-9305

²Joint Astronomy Centre, National Research Council Canada, 660 N. A'ohoku place, University Park, Hilo, HI 96720

³University of Toronto, Department of Astronomy and Astrophysics, 60 St. George Street, Toronto, ON, M5S 3H8, Canada

in mergers of gas-rich systems (see Sanders & Mirabel 1996 for a review), some gas-rich interacting galaxies that are yet not very infrared-luminous or active in star formation still lack thorough investigation. Why the interaction or merging in some gas-rich galaxy pairs does not instantaneously lead to the luminous starburst phase remains elusive.

The Taffy galaxies (UGC 12914/15, VV 254), comprise an extraordinarily gas-rich pair with $M(\text{HI}) \sim 1.5 \times 10^{10} M_{\odot}$ ⁴ (Mirabel & Sanders 1988; Condon et al. 1993) and $M(\text{H}_2) \sim 4.5 \times 10^{10} M_{\odot}$ (this work, also Smith & Struck 2001). The total molecular gas mass in this system, derived using the standard CO-to-H₂ conversion applicable to giant molecular clouds (GMCs) in the Galactic disk, is about 3 times that of the archetypal galaxy mergers — the Antennae galaxies Arp 244 (Gao et al. 2001b; Zhu, Seaquist, & Kuno 2003) and the nearest ULIG Arp 220. But, strictly speaking, the Taffy system is not a bona-fide LIG, with only $L_{\text{IR}} = 8.1 \times 10^{10} L_{\odot}$ (see Sanders & Mirabel 1996 for the definition of L_{IR}).

Although Taffy is evidently a strongly interacting system, the global star formation efficiency, in terms of star formation rate (L_{IR}) per unit of molecular gas mass, $\text{SFE} = L_{\text{IR}}/M(\text{H}_2) \sim 2L_{\odot}/M_{\odot}$ is rather low. This is nearly 10 times lower than that of most LIGs (Gao & Solomon 1999), which are mainly interacting gas-rich galaxy mergers. In this regard, Taffy is also similar to the Antennae galaxies (Gao et al. 2001a) and a few known LIGs with lowest SFE, coldest far-IR colors, and abundant cold dust/gas, such as Arp 302 (Gao 1996; Lo, Gao, & Gruendl 1997), for example. How does the Taffy system retain globally most of the gas not actively forming into stars? Is the SFE really low or is the CO-to-H₂ conversion factor X well off-scale, resulting in a serious overestimate of the molecular gas mass? Are there any starbursts going on at all? Where are the starburst sites?

The Taffy pair is remarkable, however, in that large amounts of radio continuum emission are found between the galaxy disks, connecting the two galaxies in a taffy-like structure (Condon et al. 1993). HI is also mostly distributed between the

two galaxies in the taffy bridge (Condon et al. 1993), rather than in the spiral disks or the tidal tails. The Taffy not only shows an unusual HI morphology, but also the HI kinematics indicate two fast counter-rotating disks (rotation speed near 300 km s^{-1} , Condon et al. 1993) even after the collision. The highest HI column densities located in the taffy bridge are thus apparently a result of the stripped HI gas clouds owing to the direct cancellation of their motion after the counter-rotating, interpenetrating, and head-on disk collision. It is conceivable that some GMCs were left behind in a similar way although the chance of direct collision between GMCs is rather small (e.g., Jog & Solomon 1992).

While little emission is found in the bridge/gap region in the optical and near-infrared wavelengths, the H α image clearly reveals a distinctively separated H II region near the disk of the northeastern galaxy UGC 12915 (Bushouse & Werner 1990). This HII region is also the strongest radio continuum site in the bridge. Jarrett et al. (1999) showed that there are several vigorous star-forming regions in and near UGC 12915, based on the ISO mid-IR images, and one corresponds to this extra-disk HII region. Condon et al. (1993) also noted that synchrotron emission from relativistic electrons trapped in the bridge nearly doubles the total radio luminosity expected from spirals based on the tight far-IR/radio correlation (e.g., Helou, Soifer, & Rowan-Robinson 1985; Condon 1992). Then, the excess radio emission in the bridge may have little to do with the enhanced star formation. Is this indeed so?

There is also a ring-like pattern in the southwestern (SW) galaxy UGC 12914. The symmetric ring structure appears to be well explained by N-body simulations and is believed to be formed when the “intruder” galaxy UGC 12915 goes through the rotating disk of the “target” galaxy UGC 12914 (Appleton & Struck 1996; Gerber et al. 1990, 1996; Struck 1997). The well defined dynamical history of ring galaxies also makes the Taffy system an ideal candidate for studying the effect of galaxy interaction on the ISM and for understanding the interaction-induced star formation.

All these observations and numerical modeling are somewhat hampered by the lack of knowledge of the detailed molecular gas distribution

⁴In this paper we use the following values $d_{\text{L}} = 60 \text{ Mpc}$, $H_0 = 75 \text{ km s}^{-1} \text{ Mpc}^{-1}$

and kinematics, which are essential to understanding star formation and constructing the interaction history. Both the HI disk morphology and HI gas kinematics are too severely disturbed, and the spatial resolution is too low to deduce the detailed galaxy disk kinematics of the pre-collision spiral pair. In comparison, molecular gas disks should suffer less damage in the early stage of galaxy interactions. CO imaging can thus better probe the star-forming gas distribution and kinematics of the progenitor galaxies as well as current/future sites of star formation. Our high-resolution CO observations and multiwavelength comparisons might provide a Rosetta stone to shed light on more detailed numerical modeling incorporating the multiphase ISM (e.g., Struck 1997; Barnes 2002).

2. OBSERVATIONS

The 10-element Berkeley-Illinois-Maryland Association (BIMA) interferometer (Welch et al. 1996) is the most suitable millimeter instrument available at present to image the extended CO distribution and kinematics of the Taffy galaxies. This is because the BIMA has a large field-of-view of $\sim 2'$ at 3mm as well as short baseline u-v coverage (the shortest baseline is ~ 7 m in the ultra-compact D array configuration). In addition, the flexible correlator configuration covers a rather broad velocity range. These characteristics are ideal for mapping extended CO emission of angular extent $\gtrsim 40''$.

Also because the entire Taffy system extends over $2'-3'$, we adopted two-field mosaicing with each field-of-view's phase center pointing roughly near each galaxy's nucleus. This gives a sufficient overlap between the two BIMA pointings over the taffy bridge since the nuclear separation is $67''$, much smaller than the BIMA's primary beam (FWHM $\sim 100''$) for CO(1-0).

The observations were carried out during 1999 April—July. There were a total of 10 usable tracks accumulated for this project: 6 regular long (7–9 hrs) tracks at both the ultra-compact D and compact C array configurations, plus 4 short (4–6 hrs) tracks.

The on-source integration was equally split between the two fields after observing the nearby quasar 0010+109 several minutes for phase cali-

bration. Uranus was also observed during each track in order to calibrate the antenna gains. Observations were carried out mostly under good/fair weather conditions. Details are summarized in Table 1. Data reduction was performed mostly with Miriad. The maximum entropy method (MEM) was used only in deconvolution, although Sault et al. (1996) have implemented mosaicing algorithms which can use either CLEAN or MEM for simultaneous deconvolution.

All calibrated u-v data for the 10 BIMA tracks have been combined and inverted with the mosaic mode, and two sets of channel maps were created with velocity resolutions of 20km s^{-1} and 40km s^{-1} . The cleaned beamsize is $9.^{\circ}9 \times 9.^{\circ}7$, corresponding to natural weighting (robust=1.2) in order to maximize the signal-to-noise ratio. We also produced a high resolution datacube of uniform-weighting (robust=−1.0) with synthesized beam of $5.^{\circ}0 \times 4.^{\circ}2$, but throughout this paper we focus on the more sensitive low resolution datacube, because of their higher sensitivity and dynamic range. Further cleaning of the background noise was done in AIPS. Moment maps were then produced from the cleaned datacube. For comparison with the VLA HI results (Condon et al. 1993), we smoothed our CO datacube to the same $18''$ resolution by Gaussian convolution.

3. RESULTS AND ANALYSIS

3.1. Molecular and Atomic Gas Distribution and Masses

Figure 1 presents the velocity integrated CO intensity map (the moment zero map) in false color with the two overlapping BIMA fields. We now describe main features in the CO distribution associated with each galaxy – namely the molecular gas disks/rings and nuclear CO, the extra-disk CO concentration in the bridge coincident with the HII region, and the very extended, rather diffuse molecular gas in the taffy bridge. Both galaxies show nuclear CO concentrations, but UGC 12915 (the intruder) exhibits the strongest nuclear CO concentration. A significant quantity of CO in the bridge is associated with the HII region, which appears to be directly attached to the molecular disk of UGC 12915. This is much more clearly shown in the velocity channel maps of 20km s^{-1} width presented in Fig. 2, which will be further detailed

in the next section (§3.2). Moreover, the amount of molecular gas in the bridge between the galaxies appears to be comparable to that of UGC 12914 (target).

Fig. 3 presents the large-scale HI distribution of the Taffy system (Condon et al. 1993), with respect to the optical structures. Obviously, the highest HI concentrations are in the bridge, and quite extended, rather than associated with the disks. Furthermore, nearly half of the total HI is located between the optical disks. The white contours in Fig. 3 show the location of the HI peak as well as the half-maximum contour running through both optical disks. Unlike CO which is mostly confined to the disks, HI is mostly located in the taffy bridge and the tidal tails, presumably the effects of ram pressure and tidal stripping. In fact, the HI disk morphology of the individual galaxies has mostly disappeared although kinematically recognizable, and the two HI disks seem to have already merged into one system.

UGC 12914 has prominent stellar ring structures, which are also clearly visible in the DSS image (Figs. 2 & 3). Unlike the luminous infrared ring galaxy NGC 1144, where huge CO concentrations are distributed along the rings (Gao et al. 1997), little molecular gas is detected in the ring of UGC 12914. However, the HI brightness might peak on part of the ring, and weaker HI concentrations appear to follow the ring structures (Fig. 3), although the limited spatial resolution doesn't allow any detailed comparisons. Secondary CO concentrations are also obvious in both galaxies, most likely indicating the locations of the rotating CO rings/disks.

We estimate the CO fluxes over different regions, as well as the total CO flux of the entire system, using both the velocity integrated CO intensity (moment zero) map (Fig. 1) and the velocity channel maps (Fig. 2). From optical images, different regions such as disks, rings, and HII regions can be rather easily defined, although no distinct taffy feature is visible. The exact division of different CO regions is not well defined, however. For instance, CO emission from the extra-disk HII region is intimately connected to the CO disk of UGC 12915, which is mildly distorted. And it is difficult to assign the exact borderlines separating different regions even in the velocity channel maps (Fig. 2). In particular, the separation of the HII

region from the diffuse taffy bridge CO is arbitrary. The adopted values based on our measurements over various regions are summarized in Table 2.

It is also difficult to distinguish the extended CO bridge from the CO possibly associated with part of the ring structures and the weak CO near the strongest HI emission peak (Fig. 3), even using the CO velocity channel maps. This is partly due to the limits imposed by the spatial resolution, particularly in the HI observations, the sensitivity of our observations, and partly to the rather diffuse nature of the neutral gas (both molecular and atomic) in the bridge. Also the CO fluxes can increase by up to $\sim 20\%$ if weaker extended regions of lower signal-to-noise ratio ($\lesssim 3\sigma$) are included.

Using the standard CO-to-H₂ conversion, $X \equiv N(\text{H}_2)/I_{\text{CO}} = 3.0 \times 10^{20} \text{ cm}^{-2} (\text{K km s}^{-1})^{-1}$, applicable to Milky Way disk GMCs, we can estimate the molecular gas mass in different regions across the system. We obtain the molecular gas mass directly from the estimated CO fluxes ($f_{\text{CO}} = \int S_{\text{CO}} dv$) in Table 2, using $M_{\text{H}_2}(M_{\odot}) = 1.18 \times 10^4 D_L^2 f_{\text{CO}}$, where D_L is luminosity distance in Mpc, which is equivalent to the standard CO-to-H₂ conversion. Note the conversion from Jy/beam to Kelvin for the synthesized beam of $9.^{\circ}9 \times 9.^{\circ}7$ is $0.99 \text{ K}/(\text{Jy}/\text{beam})$. We thus obtain the total molecular gas masses of UGC 12914, UGC 12915, the HII region, and the Taffy bridge to be 1.3 , 1.5 , 0.4 , and $1.4 \times 10^{10} M_{\odot}$ respectively.

Several papers have reported single-dish CO observations of the Taffy system. Smith & Struck (2001) observed nine pointings using the former NRAO 12m telescope and yielded five detections. They reported molecular gas masses of $1.9 \times 10^{10} M_{\odot}$ and $1.7 \times 10^{10} M_{\odot}$ for UGC 12915 and 12914 respectively. An upper limit of $\lesssim 1.9 \times 10^{10} M_{\odot}$ was also given for the taffy bridge. Judging from the CO image, both of the 12m beams pointing at UGC 12915 and at the taffy bridge completely cover the dominant extra-disk CO feature. Thus the molecular gas mass from the taffy bridge excluding the CO concentration at the HII region should be much less than this upper limit. Overall, a total molecular gas mass of $\sim 4.5 \times 10^{10} M_{\odot}$ for the whole system seems to be in excellent agreement with our BIMA results.

Zhu et al. (1999) and Zhu (2001) also reported the total fluxes of the Taffy system based on their observations with the NRAO 12m and IRAM 30m

telescopes. Both measurements are in excellent agreement with our BIMA results. The IRAM observations (Braine et al. 2003) map the entire system at CO J=1–0 and 2–1 transitions with 11'' spacing. The comparison of the BIMA interferometer data and the IRAM single dish data shows that the BIMA map has recovered virtually all the CO flux within the calibration uncertainty of 20%. The quantitative study of the excitation of the molecular gas in this system combining the CO data at J=1–0, 2–1 and 3–2 transitions from different telescopes will be reported in a future paper (Zhu, Seaquist, & Davoust 2003).

The Taffy system was also recently observed in the sub-mm continuum by Dunne et al. (2000). The 850 μ m fluxes of UGC 12915 and 12914 were listed as 160 and 131 mJy respectively. The total dust mass estimated is close to $10^8 M_\odot$ assuming a single dust temperature, but including cold dust with $T_{\text{cold}} = 20\text{K}$ can increase the dust mass by a factor of 2 (L. Dunne 2003, private communication). Also, there may be significant diffuse emission between the galaxies which is not yet detected. Thus the actual dust mass can be much higher than the value reported above.

The H I gas mass (Table 2) can be estimated using $M_{\text{HI}}(M_\odot) = 2.36 \times 10^5 D_L^2 \int S_{\text{HI}} dv$, where $\int S_{\text{HI}} dv$ is the H I integrated flux in Jy km s $^{-1}$. We use the estimated HI fluxes from the total HI line emission map shown in Fig. 3.

For a total gas mass (both HI and H₂) of $6 \times 10^{10} M_\odot$, we expect the total dust mass to be on the order of $3 \times 10^8 M_\odot$ assuming a Galactic dust-to-gas mass ratio of 1/200.

This value, based purely on the empirical gas-to-dust ratio, thus constrains the CO-to-H₂ conversion factor X (see §4.3.1). Future more sensitive sub-mm measurements including 450 μ m with SCUBA on the JCMT, as well as SIRTF far-IR observations, will firmly settle these issues.

3.2. The Gas Kinematics

In the velocity channel maps, rather detailed radial velocity information and the kinematic relationship of the various structures can be identified (Fig. 2). The molecular gas in the SW galaxy (UGC 12914, the target) first appears at -360km s^{-1} (4040km s^{-1}) in the inner part of the hook-like structure near NW

edge of the stellar disk. With increasing velocity, CO emission shifts systematically towards SE along the stellar disk, and eventually disappears around 280km s^{-1} (4680km s^{-1}). The much stronger CO in UGC 12915 (the intruder) first becomes prominent at -200km s^{-1} (4200km s^{-1}), but may show a much fainter signature starting as low as -360km s^{-1} (4040km s^{-1}). The rather strong molecular gas concentrations in the intruder disk move with increasing velocity towards the NW, following the expected rotation pattern. The molecular gas in UGC 12915 shows a direct kinematic connection with the strongest CO concentration in the bridge, and disappears entirely beyond 420km s^{-1} (4820km s^{-1}). The high velocity CO in the intruder is associated with the dusty patches in the NW which are evident in the DSS image. This indicates the progenitor disk of the intruder is slightly more tilted, relative to the target galaxy's disk, than that which appears in the DSS image. Both the NW stellar extension and SE fainter edge are possibly related to the tidal features produced during collision. This is also evident by examining the 2MASS images, which clearly show that the underlying stellar disk of the intruder galaxy is confined to the dusty patches in the DSS image. The sense of the rotation of the two molecular gas disks is exactly opposite. Thus, both disks have molecular gas in counter-rotation at speeds exceeding 300km s^{-1} , even after the direct, interpenetrating, head-on collision.

The molecular gas in the taffy bridge has a much smaller velocity range than the velocity spread of the two counter-rotating molecular disks. Nevertheless, this material has a velocity spread of over 200km s^{-1} . The emission emerges at -60km s^{-1} (4340km s^{-1}), becomes progressively more prominent around 80km s^{-1} (4480km s^{-1}), and disappears at $\sim 200\text{km s}^{-1}$ (4600km s^{-1}). The velocity spread of the strongest CO feature in the bridge, the HII region adjacent to the intruder galaxy, is identical to that of the CO emission over the entire bridge region. These features are perhaps better represented in the first moment (velocity field) and second moment (velocity linewidth) maps shown in Fig. 4. These moment maps (Figs. 1 & 4) are derived from the detailed velocity channel maps (Fig. 2).

In summary, the CO kinematics and the overall CO morphology reveal two rapidly counterro-

tating CO disks ($\gtrsim 300 \text{ km s}^{-1}$) with a fairly large amount of extended CO emission in the bridge. The CO emission in the bridge, including the concentration at the HII region, occupies a much smaller velocity spread than the rest of the system (Fig. 4b), yet its mean velocity is about the same as the systemic velocity of the whole.

Using the convolved CO datacube (to match the $18''$ resolution of the HI), and the VLA HI datacube, kindly provided by J. Condon, we constructed the position-velocity (P-V) diagrams presented in Fig. 5a & 5c. For both galaxies, the P-V maps show that the HI and CO are distributed roughly in the same velocity range, but HI spans a much larger spatial extent. In particular, for both CO and HI along the major axes, the P-V plots clearly show the rotation pattern of the gas disks.

To reveal more clearly the difference between the HI and CO gas properties in the bridge, we also show an additional P-V diagram across the bridge (Fig. 5b). The P-axis joins the nuclei of the two galaxies, and passes through the CO concentration in the HII region. Clearly, there are two velocity components in HI at ~ 4500 and $\sim 4250 \text{ km s}^{-1}$, whereas almost the entire CO emission in the bridge has only the $\sim 4500 \text{ km s}^{-1}$ component. In addition, a clear kinematic connection between the intruder UGC 12915 and the CO in the bridge is evident from this P-V plot as the cut is roughly along the minor axis, goes through HII region and the bridge.

Evidently, CO in both galaxy disks retains the signature of the solid-body rotation pattern, whereas the HI disks are certainly distorted and/or lopsided (Fig. 5a & c). In both HI gas disks, the distortion/lopsidedness is associated with the higher velocity parts. In fact, the extended HI emission appears to be reminiscent of the long HI tidal tails observed in most galaxy mergers. In extreme cases like the Antennae galaxies, more than half of HI appears to end up in the HI tidal tails (Hibbard et al. 2001a).

The foregoing comparisons indicate that both CO disks have mostly survived the head-on collision, and retained $\gtrsim 300 \text{ km s}^{-1}$ rotation velocity (Fig. 5a & c), whereas the HI disks have been disrupted, exhibiting smaller rotation velocity than that of CO, and possessing a very asymmetric distribution, both spatially and kinematically, owing

to the strong disk collision.

In Fig. 6, the grid spectra of both CO and HI in the bridge gap also show a distinct difference: one peak for CO but a double-peak for HI. Obviously, CO is associated with the higher velocity HI component in the bridge.

From the HI channel map shown in Fig. 5 of Condon et al. (1993) and the overall HI morphology (Fig. 3), it is also evident that both of the HI disk extensions and the HI tidal tails (towards SE of the target and NW of the intruder) are in the higher velocity ranges. But, the severe damages in the HI disks are more associated with the lower velocity HI, which is now mostly in the taffy bridge. This is also clearly shown in the P-V plots (Fig. 5), particularly in the target galaxy UGC 12914, where most of lower velocity HI has been stripped away and left behind in the bridge.

From the spatial distribution of both CO and HI in the bridge, it may be seen that there is almost no CO detected coincident with the HI peak position (Figs. 1–3). This is clearly revealed from the CO (Fig. 2) and HI (Fig. 5 in Condon et al. 1993) channel maps over roughly same velocity range in the bridge. Most of CO in the bridge is in the HII region, and to the south of the HI peak, which might be related to the ring structures of the target galaxy. This is partly reflected in the P-V plot cutting through the bridge (Fig. 5b), as well as the spectra of HI and CO near HI peak (Fig. 6). Except for the HI extensions/tails associated with the tidal features in the galaxy disks, most of HI is rather extensively distributed across the bridge in two distinct velocity ranges, and possibly originates from both galaxies.

3.3. Star Formation Efficiency Map

The ratio of $L_{\text{IR}}/M(\text{H}_2)$ ($\sim 2 \text{ L}_\odot/\text{M}_\odot$ for the Taffy system) is often referred as the global star formation efficiency (SFE) since the total FIR emission, the tracer of the global star formation rate, has been normalized by the total molecular gas mass available to make stars. Similarly, we can quantify the local star formation properties by measuring the local SFE. We have localized measurements of the molecular gas mass from CO maps. We here characterize the star formation rate simply by using the radio continuum emission as a surrogate for the FIR emission (see § 4.2; also

Murgia et al. 2002). We thus obtain the radio-to-CO ratio map to reveal the variation in local SFE. A successful application of this technique to the Antennae galaxies can be found in Gao et al. (2001a). The VLA 20cm continuum (Condon et al. 1993) and our CO maps have roughly comparable spatial resolution. Thus a direct division can be obtained once the 20cm continuum map has been regridded to match the pixel scale of the CO map.

Remarkably, the local 20cm/CO ratio (Fig. 7) changes in most cases only by factors of a few and stays roughly constant over the bulk of the molecular gas distribution. The lowest contour plotted is the geometric mean of the minimum and maximum of the 20cm/CO ratio. Successive contours increase by a factor of $\sqrt{2}$. The peak contour is only a factor of 5 larger than the average. The highest SFE sites, with $\text{SFE} \gtrsim 11 \text{ L}_\odot/\text{M}_\odot$, are in the nuclear region and in the inner edges of the molecular gas ring/disk of UGC 12915. The adjacent extra-disk starburst site (the HII region) in the bridge has $\text{SFE} \gtrsim 7 \text{ L}_\odot/\text{M}_\odot$, nearly twice that of the Galactic GMCs. The inferred SFE across most of the taffy bridge is comparable to the highest found in the nuclear region of the target galaxy UGC 12914, which is about the same as that of the Galactic GMCs. The region around the highest HI peak, where little CO emission is found, has slightly higher SFE than even the nuclear region of UGC 12914.

Therefore, the sites of highest SFE are exclusively associated with the possible starburst sites in the intruder. Other plausible active star-forming sites of modest SFE are perhaps in the taffy bridge, one at the HII region, and the other near the highest HI column density. The other regions in the taffy bridge as well as the target galaxy have normal SFE comparable to that of Galactic GMCs, and are thus just normal star-forming sites.

3.4. The Multiwavelength Comparison

Fig. 8 presents near-IR H-band, ISO mid-IR $15\mu\text{m}$ (Jarrett et al. 1999), VLA 20cm continuum, and HI line emission (Condon et al. 1993), overlaid with CO contours. Although it is quite faint, the HII region also shows up in the near-IR image (Fig. 8a). Even 2MASS images appear to indicate some faint emission at the HII region. This HII

region is also evidently present in the $15\mu\text{m}$ image (Fig. 8b), although it is not certain whether other mid-IR features in the taffy bridge are real or not.

The best match in Fig. 8 is between the radio continuum and the CO emission, including the taffy bridge. Most of the main features, either in the disks or in the taffy bridge, appear in both 20cm and CO images (Fig. 8c). However, it is noticeable that the northern portion of the taffy bridge, evident in radio continuum, is rather deficient in CO emission. The deficiency in CO in some location is likely real, in particular, some small gaps appearing in the SFE contour map (Fig. 7) due to the lack of CO emission there. Comparison between CO and HI (Fig. 8d) indicates that most of the extended HI concentrations are systematically shifted towards the NW direction relative to most CO emission in the bridge.

With all observations combined, in particular, the CO and HI kinematics, we may better constrain the various parameters of the two galaxies. Given the strong distortion of the HI morphology/kinematics, parameters like the maximum corrected rotation velocity V_{max} at radius R_{max} are better deduced from CO data. This is because the molecular gas disks have suffered less disruption than the HI disks. Furthermore, the inclination of UGC 12915, determined from the near-IR morphology, is slightly less than that apparent in the optical image (Fig. 6a). The tidal feature elongated towards the NW leads to slightly higher estimate of the inclination. Compared with published values (Giovanelli et al. 1986) we use an inclination of $\sim 70^\circ$ rather than 73° for UGC 12915, and 61° for UGC 12914, identical to the previously published value.

The observed CO velocity linewidths are $W = 600\text{km s}^{-1}$ and 580km s^{-1} , for UGC 12915 and UGC 12914 respectively, and thus $V_{\text{max}} = 315\text{km s}^{-1}$ and 327km s^{-1} after the inclination and redshift broadening corrections. In comparison, the HI linewidths of 510km s^{-1} and 550km s^{-1} , $V_{\text{max}} = 260\text{km s}^{-1}$ and 310km s^{-1} were given for UGC 12915 and UGC 12914 respectively by Condon et al. (1993). Note that the value of R_{max} estimated from HI data might be too large owing to the contamination by the HI tidal features. Therefore, we use CO data which give $R_{\text{max}} = 0.41'$ and $0.25'$ to estimate the dynamical masses of UGC 12914 and UGC 12915, which are

4.5 and $2.6 \times 10^{11} M_{\odot}$ respectively.

4. DISCUSSION

4.1. The Gas Pile-up and Dynamics in the Taffy Bridge

When two counter-rotating gas disks collide at high speed, the diffuse gas clouds (mainly HI) collide at highly supersonic speeds. Thus, we can expect an extensive “gas splash”, and possibly other observable effects of shock heating and radiative cooling as probed by numerical simulations (Struck 1997; Barnes 2002). The Taffy system is particularly unique, with a nearly face-on collision, and the relative collision speed of HI clouds is nearly 900 km s^{-1} , since the estimated transverse collision speed of the two galaxies is about 600 km s^{-1} (Condon et al. 1993). The velocities of the HI clouds could be essentially canceled after a direct, counter-rotating, and dissipative head-on collision. Apparently, the molecular gas disks have mostly survived the collision. The HII region, however, may have been recently formed out of the extra-disk molecular gas concentration that has been pulled out of the molecular gas disks and condensed after the collision.

A simple estimate can be made for the amount of HI left in the taffy bridge. For a perfect face-on disk collision with same counter-rotating speed, all HI clouds in two galaxies that have collided inelastically will be left behind after collision. Essentially almost all diffuse gas could be pulled out of the disks when the collision velocity is much smaller than the rotation speed. When the collision speed is much larger than the rotation speed, however, the amount of gas that collides will be less, depending upon the exact area of the disk-to-disk overlap and the amount of area of the disks that has been swept owing to the counter-rotation during their close impact. The Taffy system falls between the two extreme cases as the collision speed is comparable to the counter-rotating speed.

Judging from the multi-wavelength images, particularly the radio continuum and HI maps compared to CO (Fig. 8), the intruder may have collided with the inner nuclear region and the entire NW portion of the target disk with an angle of nearly 30° between the major axes. According to Toomre & Toomre (1972), the impact parameter should be smaller than the disk radii in order

to produce the ring structures, rather than the prominent tidal tails. However, there are weak tidal features present. Thus the impact parameter can't be much smaller than the disk radii either, since numerical simulations show that encounters with impact parameter larger than the galactic radii can be most effective in producing long tails and stronger gas inflow toward the nuclei. Given these considerations, most of the SE portion of the target disk might be much less damaged. A small portion of the intruder's HI disk in the NW may have suffered less impact as well, owing to this particular impact configuration. Judging from the HI distribution in Fig. 3, we can assume that more than $1/3$ of HI clouds in the target galaxy reside in the SE disk and about $1/3$ of HI gas in the intruder galaxy is located in its NW disk. Then most of HI in the intruder and the HI in the NW portion of the target galaxy, totalling about half of the total HI gas of the system, could have experienced a collision, owing to the sweeping of the counter-rotating disks, with the remnants mostly left behind in the taffy bridge. A direct comparison of the HI morphology with the CO image and the stellar disks (Fig. 8) appears to indicate that indeed nearly $\sim 50\%$ of HI is located in the taffy bridge between the two disk galaxies.

Our BIMA CO maps obviously reveal abundant H_2 gas in the bridge. In particular, there is a high concentration of molecular gas near the intruder, coincident with the $\text{H}\alpha$ source, indicating clearly an active extra-disk star-forming region. The spatial distribution and kinematics of CO along the bridge suggest that most CO is, in fact, the gas splash following the interpenetration of two inner molecular disks. Interestingly, except for the ring structures and the molecular gas concentration in the HII region, little on-going star formation is detected in the bridge. The dust extinction, resolution, and sensitivity could all be the contributing factors for detecting few stars. Although the peak HI column density at the taffy bridge is only $3 \times 10^{21} \text{ cm}^{-2}$, as measured by VLA $18''$ beam, the CO emission observed by the BIMA $10''$ beam in the bridge actually dominates the column densities (using the standard CO-to- H_2 conversion factor). The lowest column densities in the bridge detected in CO are in fact several times larger than the peak HI column density. The estimated extinction near the HI peak region, where the CO is weakest, could

still be quite high, with $A_V \gtrsim 10$ magnitudes.

Besides the obvious starburst site of the HII region in the bridge, the huge amount of HI piled up between the two galaxies could be the potential sites for the development of the overlapping starbursts which are quite common in interacting galaxies (Xu et al. 2000). Such large HI gas concentrations are also found in galaxies of different interaction geometry, e.g., NGC 6670 which involves an edge-on collision (Wang et al. 2001). It is conceivable that once the HI concentrations further condense, and perhaps form into self-gravitating systems, they could capture some GMCs passing by, and could also possibly convert some HI into molecular form. An extreme example with prominent overlapping starbursts is the Antennae galaxies, where more than 50% of the total CO emission is found in the overlap region (Gao et al. 2001a). In the Taffy system, the huge HI concentration between galaxies might then provide a mechanism for an eventual molecular concentration in the bridge region.

High speed (900 km s^{-1}) gas cloud collisions should produce shockwaves heating the gas to more than 10^7 K . It would be interesting to map the hot ISM of the taffy bridge and further compare the gaseous structures of different phases of ISM. The Taffy system appears to be an intermediate example, bridging the slow-speed ($\sim 300 \text{ km s}^{-1}$ or less) gas-rich merging galaxies and the very high-speed ($\sim 1000 \text{ km s}^{-1}$) encounters in compact groups of galaxies. In most merging systems, HI appears to roughly follow the distribution of the stars during the encounter, whereas huge HI reservoirs, located far away and completely outside of the galaxy disks, can often be found in compact groups of galaxies (e.g., HCG 92, Williams, Yun & Verdes-Montenegro 2002). Also in HCG 92, CO is found in the surrounding IGM HI concentrations (Gao & Xu 2000; Lisenfeld et al. 2002). Prominent large-scale $\text{H}\alpha$ and soft X-ray emission, presumably related to the HI splashes and shockwave heating, are also evident in HCG 92 (Trinchieri et al. 2003).

4.2. Star Formation across the Taffy Bridge between the Galaxies

It is tempting to interpret the 20cm-to-CO ratio as an SFE map (Fig. 7). This is because the radio continuum emission can be used as a

tracer of the recent star formation in galaxies (e.g., Condon et al. 1996; Condon 1992). In particular, there is an excellent correlation between the FIR and radio continuum emission (Helou et al. 1985; Condon 1992; Xu et al. 1994; Yun, Reddy, & Condon 2001), and the tight FIR/radio correspondences appear also to be valid at least on kpc scales in galaxies (e.g., Marsh & Helou 1995; Lu et al. 1996). Murgia et al. (2002) analyzed the 20cm/CO ratio in a large sample of star-forming galaxies and showed that it remains constant within a factor of 3 (with a resolution of about $50''$), both inside the galaxies and from galaxies to galaxies. Nevertheless, it is still debatable whether the radio continuum emission in the taffy bridge is a good indicator of star formation. Condon et al. (1993) noted that the synchrotron emission from relativistic electrons trapped in the bridge nearly doubles the total radio luminosity expected from normal spirals. Thus it is possible that the star formation rate estimated from the radio continuum could be overestimated at most by a factor of two since synchrotron emission from relativistic electrons accelerated in gas collision shocks may contribute a significant fraction of the radio continuum. The close correlation between CO and radio continuum, particularly in the extended taffy bridge (Fig. 8c), however, may imply that most of the radio continuum emission could still be related to the very recent on-going star formation (e.g., Murgia et al. 2002). The radio continuum might be directly associated with the various by-products of the star formation process, such as supernovae remnants, and is therefore still a useful indicator of the (far-IR) star formation.

The gas ($\text{HI} + \text{H}_2$) surface density in the bridge is significantly higher than the threshold for star formation as suggested by the spatially resolved study of normal spirals (Martin & Kennicutt 2001). The HI gas alone in the bridge, as mapped by the $18''$ VLA beam, is about $20 \text{ M}_\odot \text{ pc}^{-2}$ (the second white contour outlining the HI gas between the two galaxies in Fig. 3). The H_2 gas surface density is much higher, and the minimum detected by the $9.''9 \times 9.''7$ beam, using a standard conversion factor X , is as large as $150 \text{ M}_\odot \text{ pc}^{-2}$. Therefore, essentially all regions with CO detection have molecular gas surface density about one order of magnitude above the mean star forma-

tion threshold in normal spiral galaxies. It should be noted that the HI peak region could be the overlap of two HI arms (one arm from UGC 12915 and the other from UGC 12914), given the two distinctively different velocities in the bridge (Fig. 6). The actual HI column density at the HI peak regions could thus be a factor of two lower. However, the combination of the HI and H₂ (even with a conversion factor X ten times smaller) still yields a gas surface density higher than the threshold for star formation in normal galactic disks.

4.3. Is the Taffy System in a Starburst Phase?

Star formation occurs within GMCs, especially the dense cores where stars are forming with SFE orders of magnitude higher than the average. Interestingly, local starburst galaxies have SFE higher (by factors of 2–5) than normal spirals, whereas almost all LIGs/ULIGs have SFE $\gtrsim 20$ L_⊙/M_⊙, or even orders of magnitude higher than normal spirals (Sanders & Mirabel 1996). However, there are some early stage premerging LIGs with SFE ~ 10 L_⊙/M_⊙ and lower, such as Arp 302 (Gao 1996; Lo et al. 1997). Across most of the active star-forming regions in the Taffy system, however, starbursts are not particularly strong. Apart from the nuclear region of the intruder and its edge-brightened inner CO disk/ring, the HII region in the bridge barely qualifies as a true starburst site simply based on its SFE. Since the average SFE of the Galactic disk GMCs is a factor of 2 higher than the global SFE of the Taffy system, the entire system seems not to be a starburst at all. Unless we have seriously overestimated the molecular gas mass by using the standard CO-to-H₂ conversion, almost all molecular gas in taffy bridge and in the target galaxy has low SFE, and is not in the starburst phase.

The same argument may apply to both the intruder and the target galaxies as well since much smaller molecular gas mass will result in extremely high SFE, which appears also to be inappropriate. In particular, because the Taffy system is itself not a genuine LIG system yet. The tight correlation between radio continuum and CO may actually indicate that the bulk of radio continuum emission in the taffy bridge is probably related to the globally normal star formation. And it is the large scale star formation in addition to some localized

modest starbursts that power most of the energy output in the Taffy system.

4.3.1. Effect of the CO-to-H₂ Conversion Factor

Any reduction of the conversion factor X in the Taffy system will result in an enhanced SFE by the same factor. If we sufficiently overestimate the molecular gas mass in the intruder, then the intruder could clearly be a strong starburst. Similarly, if a smaller conversion factor X is used in the bridge, the molecular gas there could then be forming into stars with elevated SFE as well, even after lowering the star formation rate by a factor of 2 to bring it in line with the FIR/radio correlation. It is important to note in this context that the conversion factor X in ULIGs is significantly lower than in Galactic GMC's. In a ULIG, however, extremely high nuclear gas concentrations around the merged double-nucleus have resulted in such extraordinarily high molecular gas density that even the intercloud medium is molecular. Thus, most of CO detected in ULIGs is not from self-gravitating GMCs. Nevertheless, even under such extreme conditions, the reduction in the conversion factor X is only a factor of ~ 5 (Downes & Solomon 1998). Judging from the comparatively lower CO concentrations in the target galaxy UGC 12914, it is unlikely that such an overestimation of molecular gas occurs in this galaxy. However, this could be the case in the intruder galaxy where CO is rather highly concentrated.

However, given the mostly low concentrations of CO and lack of independent evidence for high star formation activity, it is unlikely that we have overestimated the molecular gas mass by large factor, and we conclude that star formation is probably rather inactive over bulk of the molecular gas in the Taffy system.

4.4. The Taffy Galaxies as a Future Starburst System

Like the Taffy system, many interacting systems show little or no enhanced new star formation, while statistically as a whole, they only show a factor of 2 enhancement compared to normal spirals (Xu & Sulentic 1991). Half of an objectively selected sample of 8 interacting systems imaged by ISOCAM show no particularly obvious starbursts (Xu et al. 2000). It is not surprising that high-

speed splashes and shockwave heating may inhibit star formation since they disrupt disk clouds, and lead to an overall rarefaction of disk gas, and thus only some regions that have built up enough gas concentrations can actually be actively forming into stars, and are thus in a starburst phase.

Yet it seems clear that interaction as well as the associated gas-infall and high-pressure compression of GMCs (e.g., Jog & Solomon 1992) are important for triggering enhanced star formation, though it may only be preferred in mergers with a relatively slow-speed encounter. In any case, it appears that such high-pressure compression might only be the initiator of a multi-step process. The Taffy system could have just experienced a strong starburst phase a few tens million years ago ($S_{\text{nuclear separation}}/V_{\text{transverse}} \sim 3 \times 10^7 \text{ yrs}$) at the closest splash of the two disks. We could perhaps also expect a future starburst once the two galaxy disks collide/splash again and eventually merge into one system. The molecular gas in the bridge is on average forming stars at a rate of $\sim 6 M_{\odot}/\text{yr}$ ($L_{\text{IR}} = 3.4 \times 10^{10} L_{\odot}$). It has potential for future starburst with ten-fold increase of L_{IR} in the next few tens million years as the gas depletion time is more than 2 Gyr.

4.5. Uniqueness of the Taffy Phenomenon and High-redshift Implications

Recently a second taffy pair VV 769 = UGC 00813/6 was discovered (Condon, Helou & Jarrett 2002), and the radio continuum and HI line images show many similarities with that of UGC 12915/4. This is remarkable since such systems indeed seem to be rare in the local universe (Condon et al. 2002). Nevertheless, systems with a radio continuum emission bridge between the two galaxies do exist, e.g., Arp 270 (NGC 3395/6) observed by Huang et al. (1994), although they are not as dramatic as the prominent taffy bridge in UGC 12915/4. On the other hand, a substantial population of IR luminous galaxies with dust much cooler than the local LIGs may exist at moderate/high redshifts (Chapman et al. 2002). There is also some indication that there may be a high redshift population of sub-mm sources with excess radio emission compared to the IR/radio correlation for local galaxies. Taffy does have excess radio continuum emission in the bridge and perhaps the conditions required to produce a taffy-

type system may have occurred more often at high redshift where collisions between gas-rich systems are believed to be much more frequent. In particular, its spectral energy distribution (SED) peaks beyond $100 \mu\text{m}$ suggesting a huge amount of cold dust in the Taffy system. In this sense, it is crucial to obtain a highly spatially resolved $450 \mu\text{m}$ SCUBA map and future SIRTF 70 and $160 \mu\text{m}$ maps in order to fully investigate SED across different regions in the Taffy galaxies. The study of the Taffy-like galaxies and better characterization of their SED may thus be relevant to the high- z SCUBA sources.

It is also interesting to note that the target galaxy is a ring galaxy. Thus, the Taffy system is probably at least a remote relative of galaxies in the “Sacred Mushroom” class of ring galaxies (Arp & Madore 1987). A Sacred Mushroom, e.g., AM 1724–622 (Wallin & Struck-Marcell 1994), is defined by a stem (intruder) consisting of an edge-on or disrupted companion connected to a ring galaxy forming the cap of the mushroom (target). An HI image of AM 1724–622 (also known as ESO 138 - IG 029/30) clearly shows the HI bridge (Higdon et al. 2001). The intruder’s orientation is different in the Taffy system as compared to the companion of the Sacred Mushroom ring galaxies. The fact that the two galaxies are still in contact implies that the collision is not quite over. Therefore, most of active star forming regions in the taffy bridge must be fairly young and very recent.

Arp 284 (NGC 7714/5) may provide a better example. The recent high-resolution HI observations (Smith, Struck & Pogge 1997) show that the bridge gas and HII regions are both spatially offset from the stellar bridge by a large amount. According to models by Smith & Wallin (1992) and Smith et al. (1997), the bridge may be the result of the combined action of gravitational (tidal bridges) and hydrodynamic (purely gaseous splash bridges) processes. Most ring galaxies like the Cartwheel and VII Zw 466 have gaseous splashes connecting the companion to the target ring galaxy (Higdon 1996; Appleton, Charmandaris & Struck 1996). However, the amount of HI in the bridge is small. The large amount of HI gas in the taffy bridge shows how effective these processes can be in some cases.

Although the NRAO VLA sky survey (Condon et al. 1998) found only one other taffy system

in the nearby universe, taffy phenomena exist in other forms of ISM besides relativistic particles responsible for radio continuum emission. For instance, II Zw 71 (UGC 9562) has been classified as a “probable” polar ring galaxy. However, it is connected with its companion galaxy II Zw 70, a blue compact dwarf galaxy separated by a projected distance of 23 kpc, by a taffy-like HI bridge with no detectable radio continuum emission (Cox et al. 2001). Duc et al. (2000) presented another case (Arp 245) where two galaxies are connected in HI. Quite a few more examples of HI bridges are listed in the HI Rogues Gallery (Hibbard et al. 2001b), e.g., NGC 3424/30 (Nordgren et al. 1997a) and NGC 7125/6 (Nordgren et al. 1997b). It is possible that weak extended radio continuum could exist in these taffy-like HI bridges, which requires much deeper and sensitive continuum imaging to probe. Nevertheless, little star formation is occurring in most of the HI bridges since apparently the collision damage to the molecular gas disks is minimum and few GMCs were pulled out of the molecular gas disks. It is worth noting that none of the examples mentioned are LIGs, although most have a large gas reservoir (at least HI).

Other cases exist with radio continuum emission outside of the galaxy disks, but not necessarily located exactly between the merging disks. In NGC 6670 (Wang et al. 2001), a huge HI gas concentration is found between the two merging disks of heavily distorted HI morphology. But the nearly edge-on merging geometry seems to produce an extra-disk HI overlap which is not exactly between the nuclei. Weak radio continuum is also apparent in the HI concentration outside of the disks of NGC 6670. In the “Antennae” galaxies, the dominant radio continuum emission is also from the overlap region (Neff & Ulvestad 2000; Gao et al. 2001a), which is not exactly between the two nuclei. II Zw 96 also exhibits dominant radio continuum (Condon et al. 1996; Goldader et al. 1997) where the strongest CO emission is found entirely outside of the two merging stellar disks, and also far away from the region between the two galaxies (Gao et al. 2001b). It is difficult to understand how collision/merging could produce so much gas and star formation outside of the disks, and offset far away from the region between the two galaxies. Nonetheless, these systems with extreme offsets in the gas overlap tend

to be indeed bona-fide LIGs.

5. CONCLUSIONS

We presented two-field mosaicing CO images of the Taffy system, and compared the BIMA CO images with various observations at other wavebands. In particular, we investigated the star formation efficiency (SFE) across the entire system, including the prominent taffy bridge, to identify the starburst sites. The detailed molecular gas distribution and kinematics provide useful constraints on the orbital geometry and impact parameters of the interaction. We summarize our main results as follows:

1. Large amounts of molecular gas were clearly detected throughout the taffy bridge between the two galaxies. The highest CO concentration in the taffy bridge corresponds to the extra-disk H α source (HII region), also the strongest radio continuum source. The molecular gas mass in the taffy bridge amounts to $1.4 \times 10^{10} M_{\odot}$, using the standard Galactic CO-to-H $_2$ conversion.
2. The overall CO distribution of the entire system, including the taffy bridge, agrees well with that of the radio continuum emission, and argues for star formation as the origin of most of the radio continuum emission. We further show that the starburst sites are exclusively in the intruder galaxy UGC 12915 and the adjacent extra-disk H α source in the taffy bridge. Most of the molecular gas in the taffy bridge is forming into stars at SFE comparable to that of the target galaxy, and similar to that in Galactic disk GMCs. These are derived based on the 20cm-to-CO ratio (SFE) maps.
3. Compared to the HI morphology and kinematics, which are strongly distorted owing to the high-speed collision, CO better defines the orbital geometry and impact parameter of the interaction as well as the disk properties. The two spiral disks are clearly counter-rotating at speeds above 300 km s^{-1} . The intruder’s major axis is more tilted relative to that of its companion than inferred from its optical appearance, which is heavily affected by the dust obscuration and tidal features.
4. CO observations and a multiwavelength comparison demonstrate that the high-speed counter-rotating collision lead to the observed gas (mostly HI, some H $_2$) pile-up between the galaxies.

The impact parameter must be smaller than the disk radii so that the GMCs in the inner disks and nuclear regions have had more chance to collide during the interaction.

We thank Jim Condon, Tom Jarrett, and George Helou for providing digital images and helpful discussions. YG was supported by the NSF grant AST 01-00793 funded at the FCRAO. This research was supported in part by a research grant to ERS from the Natural Sciences and Engineering Research Council of Canada.

REFERENCES

Appleton, P.N., Charmandaris, V., & Struck, C. 1996, ApJ, 468, 532

Appleton, P.N., & Struck, C. 1996, Fund. Cosmic Phy., 16, 111

Arp, H.C., & Madore, B.F. 1987, A Catalog of Southern Peculiar Galaxies and Associations, Cambridge University Press

Barnes, J.E. 2002, MNRAS, 333, 481

Braine, J., Davoust, E., Zhu, M., Lisenfeld, U., Motch, C., & Seaquist, E.R. 2003, A&A, in press

Bushouse, H.A., & Werner, M.W. 1990, ApJ, 359, 72

Chapman, S.C., Smail, I., Ivison, R.J., Helou, G., Dale, D.A., & Lagache, G. 2002, ApJ, 573, 66

Condon, J.J. 1992, ARA&A, 30, 575

Condon, J.J., Helou, G., Sanders, D.B., & Soifer, B.T. 1993, AJ, 105, 1730

Condon, J.J., Helou, G., Sanders, D.B., & Soifer, B.T. 1996, ApJS, 103, 81

Condon, J.J., Cotton, W.D., Greisen, E.W., Yin, Q.F., Perley, R.A., Taylor, G.B., & Broderick, J.J. 1998, AJ, 115, 1693

Condon, J.J., Helou, G., & Jarrett, T.H. 2002, AJ, 123, 1881

Cox, A.L., Sparke, L.S., Watson, A.M., & van Moorsel, G. 2001, AJ, 121, 692

Downes, D., & Solomon, P.M. 1988, ApJ, 507, 615

Duc, P.-A., Brinks, E., Springel, V., et al. 2000, AJ, 120, 1238

Dunne, L., Eales, S.A., Edmunds, M.G., Ivison, R.J., Alexander, P., Clements, D., 2000, MNRAS, 315, 115

Gao, Y. 1996, Ph.D. thesis, State Univ. New York at Stony Brook

Gao, Y., Solomon, P.M., Downes, D., & Radford, S.J.E. 1997, ApJ, 481, L35

Gao, Y., & Solomon, P.M. 1999, ApJ, 512, L99

Gao, Y., & Xu, C. 2000, ApJ, 542, L83

Gao, Y., Lo, K.Y., Lee, S.-W., & Lee, T.-H. 2001a, ApJ, 548, 172

Gao, Y., Goldader, J.D., Seaquist, E., & Xu, C. 2001b, in *Science with the Atacama Large Millimeter Array*, ASP Conf. 235. ed. A. Wootten, 321

Gerber, R.A., Lamb, S.A., Miller, R.H., & Smith, B.F. 1990 in *Dynamics and Interactions of Galaxies*, ed. by R. Wielen (Springer: Berlin), 223.

Gerber, R.A., Lamb, S.A., & Balsara, D.S. 1996, MNRAS, 278, 345

Giovanelli, R., Haynes, M.P., Myers, S.T., & Roth, J. 1986, AJ, 92, 250

Goldader, J.D., Goldader, D.L., Joseph, R.D., Doyon, R., & Sanders, D.B. 1997, AJ, 113, 1569

Helou, G., Soifer, B.T., & Rowan-Robinson, M. 1985, ApJ, 298, L7

Hibbard, J.E., van der Hulst, J.M., Barnes, J.E., & Rich, R.M. 2001a, AJ, 122, 2969

Hibbard, J.E., van Gorkom, J.H., Rupen, M.P., & Schiminovich, D. 2001b, in *Gas and Galaxy Evolution*, eds. J.E. Hibbard, J.H. van Gorkom, M.P. Rupen, ASP Conf. Series, 240, 659

Higdon, J.L. 1996, ApJ, 467, 241

Higdon, J.L., et al. 2001, in *Gas and Galaxy Evolution*, eds. J.E. Hibbard, J.H. van Gorkom, M.P. Rupen, ASP Conf. Series, 240, 860

Huang, Z.-P., Yin, Q.-F., Saslaw, W.C., & Heeschen, D.S. 1994, ApJ, 423, 614

Jarrett, T.H., Helou, G., Van Buren, D., Valjavec, E., & Condon, J.J. 1999, AJ, 118, 2132

Jog, C.J., & Solomon, P.M. 1992, ApJ, 387, 152

Lisenfeld, U., Braine, J., Duc, P.-A., Leon, S., Charmandaris, V., & Brinks, E. 2002, A&A, 394, 823

Lo, K.Y., Gao, Y., & Gruendl, R.A. 1997, ApJ, 475, L103

Lu, N.Y., et al. 1996, A&A, 315, L153

Marsh, K.A., & Helou, G. 1995, ApJ, 445, 599

Martin, C.L., & Kennicutt, R.C. 2001, *ApJ*, 555, 301

Mirabel, I.F., & Sanders, D.B. 1988, *ApJ*, 335, 104

Murgia, M., Crapsi, A., Moscadelli, L., & Gregorini, L. 2002, *A&A*, 385, 412

Neff, S.G., & Ulvelstad, J.S. 2000, *AJ*, 120, 670

Nordgren, T.E., Chengalur, J.N., Salpeter, E.E., & Terzian, Y. 1997a, *AJ*, 114, 77

Nordgren, T.E., Chengalur, J.N., Salpeter, E.E., & Terzian, Y. 1997b, *AJ*, 114, 913

Sanders, D.B., & Mirabel, I.F. 1996, *ARA&A*, 34, 749

Sault, R.J., Staveley-Smith, L., & Brouw, W.N. 1996, *A&AS*, 120, 375

Smith, B.J., & Struck, C. 2001, *AJ*, 121, 710

Smith, B.J., Struck, C., & Pogge, R. 1997, *ApJ*, 483, 754

Smith, B.J., & Wallin, C. 1992, *ApJ*, 393, 544

Struck, C. 1997, *ApJS*, 113, 269

Toomre, A., & Toomre, J. 1972, *ApJ*, 178, 623

Trinchieri, G., Sulentic, J., Breitschwerdt, D., & Pietsch, W. 2003, *A&A*, 401, 173

Wang, W.-H., Lo, K.Y., Gao, Y., & Gruendl, R.A. 2001, *AJ*, 122, 140

Wallin, J.F., & Struck-Marcell, C. 1994, *ApJ*, 433, 631

Welch, W.J., et al. 1996, *PASP*, 108, 93

Williams, B.A., Yun, M.S., & Verdes-Montenegro, L. 2002, *AJ*, 123, 2417

Xu, C., Lisenfeld, U., Volk, H.J., & Wunderlich, E. 1994, *A&A*, 282, 19

Xu, C., & Sulentic, J.W. 1991, *ApJ*, 374, 407

Xu, C., Gao, Y., Mazzarella, J., Lu, N.Y., Sulentic, J.W., & Domingue, D.L. 2000, *ApJ*, 541, 644

Yun, M.S., Reddy, N.A., & Condon, J.J. 2001, *ApJ*, 554, 803

Zhu, M., Seaquist, E.R., & Kuno, N. 2003, *ApJ* 588, 243

Zhu, M., Seaquist, E.R., & Davoust, E. 2003, in preparation

Zhu, M., Seaquist, E.R., Davoust, E., Frayer, D.T., & Bushouse, H.A. 1999, *AJ*, 118, 145

Zhu, M. 2001, Ph.D. thesis, Univ. Toronto

TABLE 1
LOG OF THE BIMA CO(1-0) OBSERVATIONS IN THE TAFFY GALAXIES

#	Obs. Date 1999	Array Config.	Track Duration Hours	T_{sys} K	# of Antennas	Grades ^a
1	Apr 27	C	7.9	290±70	10	B-
2	Apr 29	C	8.0	310±70	10	B-
3	May 6	C	4.0	330±60	9	C
4	Jun 5	C	9.0	400±110	10	B-
5	Jun 14	C	6.7	300±70	10	B
6	Jul 12	D	7.0	340±80	7	C
7	Jul 14	D	5.6	380±90	7	C
8	Jul 15	D	4.5	360±90	10	B
9	Jul 19	D	5.5	320±70	9	B
10	Jul 27	D	7.5	290±80	10	B+

^aOverall grading based on system performance and weather conditions etc. as given by duty observers.
A: Excellent, B: Good, C: OK/usable, D: Bad, F: Failure

TABLE 2
CO MEASUREMENTS OF THE TAFFY GALAXIES

Source	f_{CO} Jykm s ⁻¹	V_{CO} ^a km s ⁻¹	$M(\text{H}_2)$ 10 ¹⁰ M _⊙	$M(\text{HI})$ 10 ¹⁰ M _⊙	M_{dust} 10 ⁷ M _⊙	L_{IR} ^b 10 ¹⁰ L _⊙	SFE ^c L _⊙ /M _⊙
U12915	355	100	1.5	0.4	5.	3.3	11
U12914	315	-60	1.3	0.5	6.	1.4	4
HII region	90	90	0.4	0.06	7
Bridge ^d	325	90	1.4	0.6	...	3.4	4
HI peak ^e	≤30	...	0.1	0.08	5

^aZero velocity corresponds to 4400 km s⁻¹

^bEstimated by roughly scaling according to the 20cm radio continuum emission

^cHighest estimated from the SFE ($=L_{\text{IR}}/M(\text{H}_2)$) map in Fig. 7

^dEntire bridge including the HII region and HI peak. But the highest SFE is referring to regions excluding the HII region and HI peak

^eHI peak region in a 18'' beam

Fig. 1.— CO(1-0) image of the Taffy system in false-color. The color ranges linearly from 37 to 170 Jy km s^{-1} per synthesized beam. The synthesized beam of $9.^{\prime\prime}9 \times 9.^{\prime\prime}7$ is shown in the lower left. The white dashed circles outline the two mosaicing fields mapped by the BIMA.

Fig. 2.— Velocity channel maps of 20 km s^{-1} width in contours overlaid on the DSS image. Top-left of each panel labels the velocity (here zero corresponds 4400 km s^{-1}). Contours start at 0.085 Jy/beam (nearly 4σ), and increase successively by a factor of $\sqrt{2}$. The last panel is the velocity integrated (over entire 800 km s^{-1} range) CO intensity map (moment zero map as in Fig. 1). Here contours start at $32.5 \text{ Jy km s}^{-1}/\text{beam}$, and increase by a factor of $\sqrt{2}$.

Fig. 3.— VLA HI intensity contour map (Condon et al. 1993) overlaid on DSS image to illustrate the various HI components. The lowest contour corresponds to column density $5 \times 10^{19} \text{ cm}^{-2}$. Successive contours increase by factors: 2, 4, 5.6, 8, 11.3, 16, 22.6, 32 (white), 38.1, 45.2 (white), 50, 55, 60, 64 (white).

Fig. 4.— (a) CO velocity field of the velocity integrated first moment map (zero corresponds 4400 km s^{-1}); (b) CO velocity linewidth map (the velocity integrated second moment map). The color bars code the velocity scale in km s^{-1} .

Fig. 5.— Position-Velocity maps. (a) Cut along the major axis of the intruder UGC 12915 from SE to NW; (b) A slice joining the two nuclei across the bridge from NE to SW; (c) Cut along the major axis of the target UGC 12914 from SE to NW. Grey-scale image and the white contours are HI of Condon et al. (1993) and the thick black contours are our convolved CO.

Fig. 6.— The DSS contours are compared to the near-IR K_s image (left) indicating the underlying stellar disk is slightly less tilted. The dash box outlines the area in the bridge within which the 7×5 grid spectra (right) at $9''$ spacing for both CO (thin line) and HI (thick line) were extracted. The labels (shown in the lowleft spectra) are only for CO flux in Jy/beam , and velocity range is 3900 to 4860 km/s .

Fig. 7.— The 20cm-to-CO ratio contours overlaid on the CO image. The 20cm-to-CO ratio could be interpreted as star formation efficiency (SFE) if the 20cm continuum is indicative of the star formation rate. The first contour corresponds roughly to $\text{SFE} \sim 2L_{\odot}/M_{\odot}$, the rest increases successively by $\sqrt{2}$.

Fig. 8.— CO contours compared to the multiwavelength images of the near-IR H-band (a, topleft), ISO mid-IR $15 \mu\text{m}$ (b, topright), VLA 20cm radio continuum (c, lowleft), and 21cm HI line (d, lowright). The CO contours of 22.5, 25, 27.5, 30, 35, 40, 50, 60, 70, 80, 90, 99% of the peak emission are plotted in all panels.

This figure "fg1.gif" is available in "gif" format from:

<http://arxiv.org/ps/astro-ph/0307490v2>

This figure "fg2a.jpg" is available in "jpg" format from:

<http://arxiv.org/ps/astro-ph/0307490v2>

This figure "fg2b.jpg" is available in "jpg" format from:

<http://arxiv.org/ps/astro-ph/0307490v2>

This figure "fg3.gif" is available in "gif" format from:

<http://arxiv.org/ps/astro-ph/0307490v2>

This figure "fg4a.gif" is available in "gif" format from:

<http://arxiv.org/ps/astro-ph/0307490v2>

This figure "fg4b.gif" is available in "gif" format from:

<http://arxiv.org/ps/astro-ph/0307490v2>

This figure "fg5a.jpg" is available in "jpg" format from:

<http://arxiv.org/ps/astro-ph/0307490v2>

This figure "fg5b.jpg" is available in "jpg" format from:

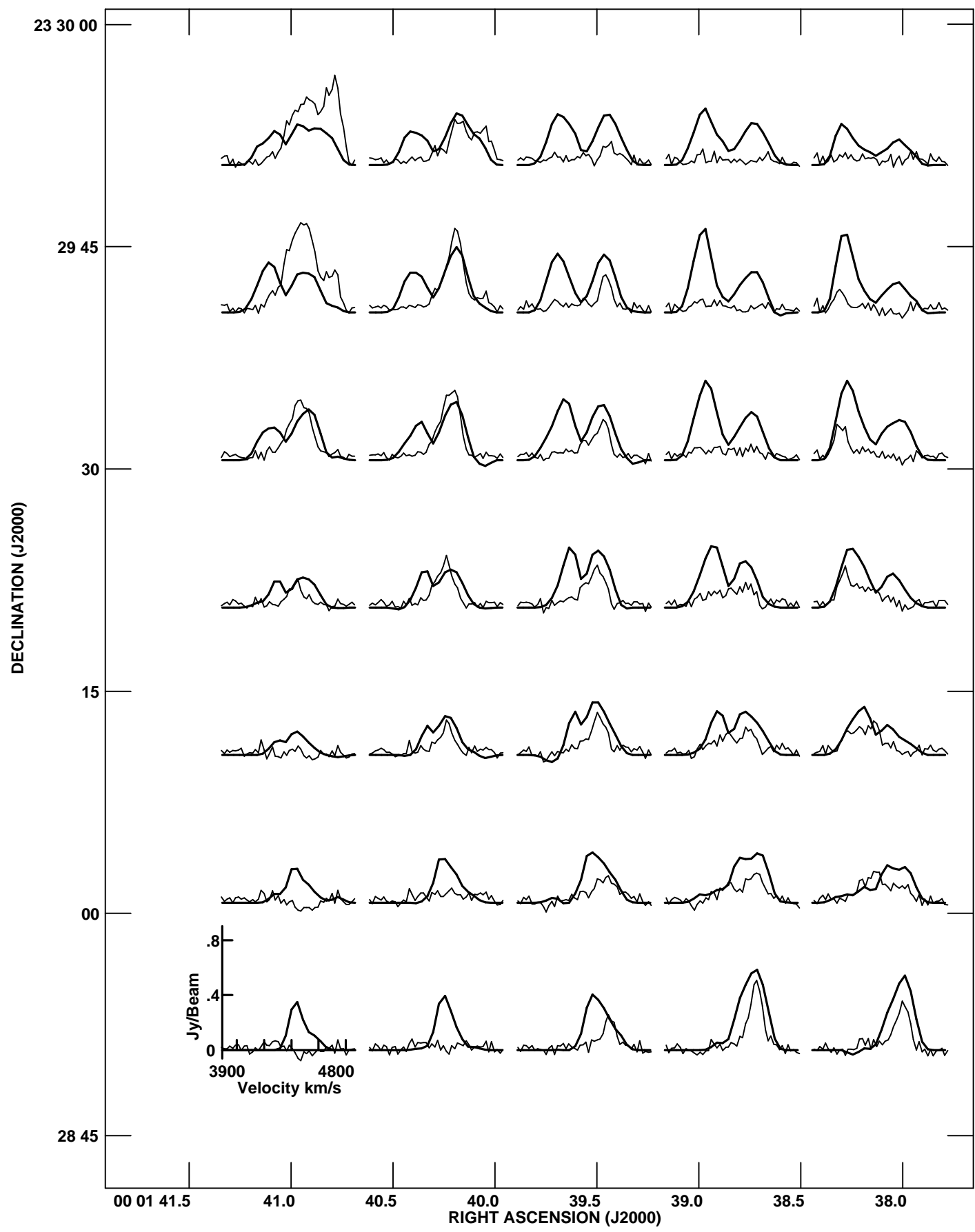
<http://arxiv.org/ps/astro-ph/0307490v2>

This figure "fg5c.jpg" is available in "jpg" format from:

<http://arxiv.org/ps/astro-ph/0307490v2>

This figure "fg6a.jpg" is available in "jpg" format from:

<http://arxiv.org/ps/astro-ph/0307490v2>



This figure "fg7.gif" is available in "gif" format from:

<http://arxiv.org/ps/astro-ph/0307490v2>

This figure "fg8a.jpg" is available in "jpg" format from:

<http://arxiv.org/ps/astro-ph/0307490v2>

This figure "fg8b.gif" is available in "gif" format from:

<http://arxiv.org/ps/astro-ph/0307490v2>

This figure "fg8c.gif" is available in "gif" format from:

<http://arxiv.org/ps/astro-ph/0307490v2>

This figure "fg8d.gif" is available in "gif" format from:

<http://arxiv.org/ps/astro-ph/0307490v2>